PCCP

Accepted Manuscript

ROYAL SOCIETY OF CHEMISTRY

www.rsc.org/pccp

The Photocatalytic Properties of Ultrathin Bismuth Oxychloride Nanosheets: a First Principles Study

Tao Jing,[a,b] Ying Dai,[*a] Xiangchao Ma,[a] Wei Wei,[a] and Baibiao Huang[a]
a School of Physics, State Key Laboratory of Crystal Materials, Shandong University, Jinan 250100, People's Republic of China
b College of Physics and Electronic Engineering, Kaili University, Kaili Guizhou 556011, People's Republic of China
*E-mail: daiy60@sina.com

Abstract

Two-dimensional (2D) nanosheet structures have obvious advantages with respect to their bulk counterparts in photocatalytic reaction due to the extraordinary electronic and optical properties. So does the 2D BiOCl nanosheets with significant improvement of photocatalytic activity in the degradation of dyes shown by recently studies. In the present work, the surface energies, electronic structure and photocatalytic properties of ultrathin BiOCl nanosheet are examined by means of density functional theory to investigate the origin of its high photocatalytic performance. The results show that Cl atom terminated BiOCl (001) surface possesses lower surface energy than others and is very likely to be introduced in the ultrathin nanosheet. Moreover, our proposed model accounts well for the origin of band edge upshift of the ultrathin BiOCl nanosheets with respect to BiOCl nanoplates observed in experiment. In addition, the presence of Bi vacancies on the surfaces of nanosheet can enhance built-in electric field and further promote the separation of photo-generated carriers, which is extremely advantageous for the photocatalytic process. Our results provide a new insight into the high photocatalytic performance of BiOCl (001) nanosheets.

1 Introduction

Semiconductor photocatalysts have been attracting tremendous attention over the past decades because of their potential in solving the global energy and environment crisis.[1-4] In terms of low toxicity and earth abundance, Bi-based photocatalytic

materials, such as Bi_2O_3, $BiVO_4$, Bi_2MoO_6 and Bi_2WO_6, have shown efficient photocatalytic performance in waste water purification and harmful pollutant removal.[5-8] Among these materials, bismuth oxychloride (BiOCl) is considered as one of the most promising candidates due to its highly efficient photocatalytic performance in the degradation of organic pollutants, which is comparable to or even better than that of anatase TiO_2.[9-12] Generally, BiOCl has the layered structure interleaved with $[Bi_2O_2]^{2+}$ slabs and double chlorine atom slabs along the [001] direction with the presence of van der Waals interaction between the two chlorine atom layers. The high photocatalytic activity of BiOCl can be assigned to the excellent separation and transfer abilities for charge carriers as the results of layered crystal structure and the presence of built-in electric field vertical to the layer direction.[13-15] In spite of the great application potential of BiOCl, the utilization efficiency of solar energy is still low due to the wide band gap harvesting only UV light (3.2eV). In order to further enhance the photocatalytic activity, a variety of strategies, aiming at the extension of optical absorption range and improvement of the quantum yield, have been implemented such as extrinsic element doping, the band engineering and morphology control for this photocatalytic material.[16-23]

The synthesis of two-dimensional (2D) nanosheets is one of the effective approaches to improve the photocatalytic performance of materials because of the extraordinary electronic and optical properties different from their bulk counterparts.[24-27] Recently, 2D BiOCl nanosheets with well-defined morphology synthesized by a facet-controlled method have significant improvement of photocatalytic activity in the degradation of dyes. It was suggested that both the increased photon harvest and improved charge separation are responsible for the enhanced activity.[28-31] On the other hand, the atomic termination of the BiOCl (001) surface, which has a close connection with its photocatalytic performance, is still under controversy because all three kinds of component atoms (O, Bi, and Cl) are likely to present on the surface depending on the synthetic conditions. In addition, various reagents have been used to tune the facet and atom exposure of BiOCl nanosheets. Recently, it has been found that the BiOCl (001) single-crystalline

nanosheets could be synthesized through tuning the PH value of solution.[32] Soon after, a theoretical investigation has suggested that the surface energy of O terminated BiOCl (001) surface is much smaller than Bi-terminated case under O rich condition, and the adsorption of H atoms at the O sites could further decrease its surface energy.[33] However, the Cl terminated (001) surface was not included in the surface energy calculations. On the other hand, previous theoretical study demonstrated that halogen atom terminated (001) surfaces have the lowest surface energies for BiOX (X = F, Cl, Br and I), but the O terminated case has not been involved in this work.[34] Thus, a systematic investigation of the properties of BiOCl (001) surfaces with different atomic terminations, in particular, the surface energy, is still missing. Recently, the novel ultrathin BiOCl (001) nanosheets with average thickness of 2.7 nm were synthesized and shown significantly higher photocatalytic activity compared with BiOCl nanoplates (thickness of about 30nm), the further investigation suggested the presence of Bi vacancies in the Bi terminated surface, which can provide places for adsorption of organic dyes facilitating the self-sensitization.[35] So far, however, the origin of the extreme enhancement of photocatalytic activity for ultrathin BiOCl nanosheets to BiOCl nanoplates is not clear. In addition, it was suggested that the band edges of these nanosheets upshift over 1 eV with respect to that of nanoplates, while the band gap of this material has not obvious change relative to the bulk. Thus, this change could not be attributed to the quantum size effect. A similar situation has been found for CoO nanoparticles while the origin of such change is still unkown.[36] On the other band, previous theoretical investigations showed that the work functions of materials are strongly dependent on surface terminations.[37,38] It is hopeful that difference of band edge positions between BiOCl (001) nanosheets and BiOCl (001) nanoplates may derive from the different atomic terminations.

In the present work, to answer the issues above, the origin of significantly enhanced photocatalytic activity of the ultrathin BiOCl (001) nanosheet is systematically investigated by first-principles calculations. The results show that Cl exposed BiOCl (001) surface has the lower surface energy than others and is very likely to be introduced in this ultrathin nanosheet. The presence of Bi vacancies in the

Bi terminated surface can increase the inherent polarity of the nanosheet and lead to band blending, which facilitates the photocatalytic process. Furthermore, the upshift of band edges of the ultrathin BiOCl (001) nanosheet relative to BiOCl (001) nanoplate can be realized because of the polarity feature of this Bi vacancy contained nanosheet. Our results may provide a reasonable explanation for the recently experimental observation.

2 Calculation methods

Our calculations were performed by the generalized gradient approximation (GGA) method within the Perdew−Burke−Emzerhof (PBE) exchange-correlation functional implemented in the VASP.[39] The projector augmented wave (PAW) potentials were used for description the interaction between core and shell. The wave function was expanded on a plane-wave basis set with the cut-off energy 400eV. The convergence threshold for self-consistent energy error was set to 10^{-5} eV, all the atomic positions were fully optimized until all components of the residual forces are smaller than 0.02 eV/Å. A Gaussian smearing of 0.05 eV was used for density of states (DOS) calculations.

The calculated lattice parameters of the tetragonal BiOCl (a=b=3.907 Å and c= 7.397 Å) are slightly larger than the experimental values (a=b=3.883 Å, c=7.347 Å) with the errors well below 0.7%. In order to avoid the additional strain by lattice relaxation, the in plane lattice parameters were fixed to our DFT values in the further calculations. The surface energy calculations were performed by using the 1×1 slab model, and the structures of five BiOCl (001) surfaces with different atomic terminations (Labeled as Bi1, Bi2, O, Cl1 and Cl2) are given in Fig 2. Previous theoretical investigation has implied that the thicknesses of slabs are sufficient to reach the convergence for the surface energies.[34] A 8×8×1 k-space grid were used for structural relaxation and static calculation. A 15 Å thickness of the vacuum layer was used to avoid the interaction between repeated slabs. Here, the surface energy is determined as follow,[40]

$$E_{sur} = \frac{E_{slab} - nE_{BiOCl}^{bulk} - n_i\mu_i}{2A}$$

here, E_{slab} is the total energy of slab, E_{BiOCl}^{bulk} is the energy of per unit BiOCl in bulk, n is the number of BiOCl units contained in the slab, n_i is the number of excess atoms of species i in the slab, μ_i is the chemical potential of species i, and A represents surface area.

Next, we employ the slab models to investigate the relative stability of the ultrathin BiOCl (001) nanosheets with different atomic terminations. As shown in Fig 3, the Bi1-Bi1, Bi1-Bi2, Bi1-O, Bi1-Cl1 and Bi1-Cl2 refer to the slabs with Bi1 termination on one side while Bi1, Bi2, O, Cl1 and Cl2 termination on the other side, respectively. It is well known that the definition of the surface energy for a polar surface is difficult because of the nonequivalent terminations. Thus, we employ the cleavage energy since previous theoretical study demonstrated that it can reflect the relative stability of different slabs,[41]

$$\gamma_c = \frac{E_{slab} - nE_{BiOCl}^{bulk} - n_i\mu_i}{A}$$

where E_{slab} is the total energy of slab, E_{BiOCl}^{bulk} is the energy of per BiOCl unit in bulk, n is the total number of BiOCl units contained in the slab, n_i is the number of excess atoms of species i in the slab, μ_i is the chemical potential of species i, and A represents surface area. Note that the difference of cleavage energy with the surface energy is only lack of factor 1/2, which can be seen as the sum of the surface energies of the two nonequivalent surfaces.

3 Results and discussion

3.1 Chemical potentials

To avoid the formation of pure elemental phases for BiOCl, the chemical potentials of component elements should satisfy the following relations under thermal equilibrium growth condition,

$$\mu_O \leq 0, \mu_{Cl} \leq 0, \mu_{Bi} \leq 0$$

In order to investigate the surface and defect properties, the chemical potential ranges

of these component elements should be determined firstly. Considering that the element chemical potentials are equal between surface and bulk under the thermal equilibrium condition. Thus, their allowed ranges can be solved by the stability of bulk phase. Thereby, it is required that $\mu_{BiOCl} = \mu_{Bi} + \mu_O + \mu_{Cl}$, here, the calculated μ_{BiOCl} value is -4.13 eV. In addition, the secondary phases should be avoided for the growth of BiOCl, the following conditions should be also added.

$$2\mu_{Bi} + 3\mu_O < \mu_{Bi2O3} = -6.76\ eV$$

$$\mu_{Bi} + 3\mu_{Cl} < \mu_{BiCl3} = -4.17\ eV$$

The allowed chemical domain for BiOCl in the μ_O and μ_{Cl} plane is shown in Fig 1 (shaded region). The calculated values at four representative chemical potential points are labeled as A, B, C and D, in which A and D refer to Bi poor condition, while the B and C correspond to Bi rich condition. The chemical potentials of μ_O, μ_{Cl} and μ_{Bi} are 0, -0.75 and -3.38 eV for A condition, respectively, while -2.25, -1.88 and 0 eV for B condition, -2.74, -1.38 and 0 eV for C condition, and 0, -0.02 and -4.11 eV for D condition.

3.2 Surface energies

Insight into the relative stability between different atomic terminated BiOCl (001) surfaces can be obtained by calculation of surface energies. Thus, as shown in Fig 4a, the surface energies of the five surfaces under four specific chemical potential points are calculated. From which we can note that the Bi1 terminated (001) surface exhibits lower surface energy compared with the case of Bi2 termination under most chemical potential conditions except the C condition. It means that, therefore, Bi1 atoms are more likely to be introduced in BiOCl (001) surface with respect to Bi2 atoms under identical growth conditions. This is consistent with the experimental result that Bi1 rather than Bi2 atoms are introduced in the surfaces of the ultrathin BiOCl (001) nanosheets.[35] In addition, it is observed that the surface energy of O terminated surface is higher than that of Bi1 terminated case excluding the D condition. Although the previous theoretical studies suggested that the surface energy of O terminated

BiOCl (001) surface is lower than that of Bi terminated surface in large chemical potential range, the Bi1 terminated surface has not been involved into their calculations.[33] Moreover, the surface energy of Cl2 terminated surface is significantly lower than other surfaces under all four growth conditions, inflecting that the absence of other capping reagents, Cl2 terminated surface possesses the largest stability. This results are in good consistence with pervious theoretical reports.[34]

The next step is to examine surface atomic terminations for the ultrathin BiOCl (001) nanosheet synthesized in experiment. Therefore, the relative stability related to atomic terminations for this nanosheet should be first investigated. Experimentally, the measurement of positron annihilation spectroscopy suggested that Bi atoms are exposed onto the surfaces of the ultrathin BiOCl nanosheets.[35] Furthermore, considering that the thickness of nanosheet reaches to the atomic scale, it is very likely that Bi1 atoms are exposed on one side while Cl2 on the other side due to the high stability. To confirm this viewpoint, the cleavage energies of these BiOCl (001) nanosheets are calculated, as shown in Fig 4b. It is obvious that the formation of Bi1-Cl2 slab is indeed of energetically more favorable than other structures, irrespective of the chemical growth conditions. To further confirm this conclusion, we calculate the thicknesses of these nanosheets, as shown in Table 1, from which it is noted that the thickness of Bi1-Cl2 slab is more close to the experimental values than others. In spite of lattice parameter overestimation due to the well-known limitation of GGA, however, it is unlikely to alter our conclusions. Our results consistently indicate the presence of Cl2 atoms on the surfaces of the nanosheet, and we will use the Bi1-Cl2 structure to carry out the further investigation.

3.3 Defect formation energies

Experimentally, it has been shown that a large number of Bi and O vacancies exist on the surfaces of the ultrathin BiOCl (001) nanosheets.[35] Here, we firstly investigate which site is energetically favorable for these vacancy defects. Therefore, the 3×2 (138 atoms) Bi1-Cl2 supercell is constructed and one atom is removed from it to

investigate the defect formation energy of this nanosheet. In addition, to facilitate the comparison of the relative stabilities of one defect among different layers, we set the most stable defect site as the zero energy reference. Thus, the calculated defect formation energies are given in Fig 5. As expected, we can note that the Bi vacancy is easier to form in the Bi terminated surface compared with the inner of the slab, and the difference is more than 6 eV. The obvious difference can be attributed not only to the increased atomic relaxation around the vacancy due to the reduced coordination of surface atoms, but also to this off-stoichiometric slab model. Moreover, a similar trend can be obtained for the case of O vacancy. Therefore, our results suggest that Bi and O vacancies are more likely to present on the surface compared with the inner of the Bi1-Cl2 slab, which strongly supports the experimental observation that Bi and O vacancies are predominant on the surfaces of ultrathin BiOCl (001) nanosheets.[35] Furthermore, these vacancies could serve as absorption sites for the organic dyes, which act as sensitizer for the visible light absorption and are responsible for the enhanced visible photocatalytic activity. The lowest energy site for Cl vacancies can be found at the second Cl layer, and the difference between these Cl layers is less than 1.5 eV, which is much smaller than the case of Bi and O vacancies, indicating that the surface effects have small influence on the formation energy of Cl vacancy. In addition, we note that the formation energy of Cl vacancy in Cl terminated BiOCl (001) side is even higher than all other layers, which can also provide an explanation that the Cl2 terminated BiOCl (001) surface possesses much high stability. On the basis of above results, the presence of these vacancies, which provide a large number of activity sites, should enable the improvement of the photocatalytic activity of the ultrathin BiOCl (001) nanosheet.

3.4 Electronic structures

The calculated band gap of bulk BiOCl is 2.62eV, which is significantly smaller than the experimental values due to the general deficiency of DFT. Here, we do not include any further correction for the band gap, because we only focus on the relative

variation trend of band edge positions. In generally, the polar surface possesses a significant dipole moment perpendicular to the surface. In particular, the built-in electric field throughout the bulk is favorable for photocatalytic process because it can serve as a drive to separate the photo-generated carriers and suppress their recombination. The built-in electric field may be introduced in this ultrathin nanosheet because the two sides are anionic and cationic exposure, respectively. Therefore, to explore the position variations of band edges for different atom layers, the Bi atom layer-resolved density of states (DOS) of the defect free BiOCl nanosheet are depicted in Fig 6. Also, the O and Cl atom layer-resolved PDOS are given in supporting information (SI1 and SI2), which show the same trend as Bi atom. Thus, we only focus on the discussion of Bi atom layer-resolved PDOS in further study. It is found that the Fermi level is pinned inside the conduction band (CB) at the first Bi layer, indicating an n-type feature. This can be attributed to the excess electrons introduced by the off-stoichiometric slab model. For the second Bi layer, both the VB and CB edges have slight raise relative to the first Bi layer, and some of CB states are occupied by electrons. However, from the 3 to 8 Bi layer, the Fermi level locates at the bottom of CB, indicating almost no electron occupation at the CB states for these layers. Therefore, our results show that this slab model is totally different from the conventional polar surfaces. That is, going from the cationic terminated surface to anionic terminated surface, the band edges of different layers increase linearly because of the presence of built-in electric field inside them. We believe that the lack of the polarity for this pure nanosheet is due to the off-stoichiometric slab model, and the excess electrons resulting from the insufficient of Cl atoms can reduce its polarity.

Since both theoretical and experimental studies suggested that a large number of Bi vacancies were introduced into the Bi terminated surfaces, it is hopeful that the holes released from the Bi vacancies can compensate the excess electrons and increase the polarity of the ultrathin BiOCl (001) nanosheet. To investigate the influence of Bi vacancies on the electronic properties of the BiOCl (001) nanosheet, firstly, the electronic structures of one Bi vacancy contained BiOCl (001) nanosheet are calculated and the Bi atom layer-resolved DOS are given in Fig 6b. The presence of

some impurity states in the band gap for the first Bi layer can be ascribed to dangling bonds and surface reconstruction brought by the Bi vacancy. For the second Bi layer, only small impurity states appear in the band gap, and the VBM rises slightly. More surprisingly, we note that, going from the Bi terminated surface to the Cl2 terminated surface, the VB of Bi layers increases gradually, and the total upshift is about 0.5 eV. It means that a band bending can be realized in this BiOCl nanosheet due to the presence of built-in electric field, which can provide a driving force promoting the separation of photo-generated carriers. Previous theoretical studies suggested that the presence of a large value of dipole moment between the $[Bi_2O_2]^{2+}$ and the anionic halogen layers can suppress the recombination of photo-generated carriers.[13] However, in order to participate in photocatalytic reaction, these carriers should further be separated and migrate to the surface of nanosheet. In this Bi vacancy contained nanosheet, the band bending leaded by the macroscopic electrostatic field can drive the separation of carriers to different surfaces. That is to say that photo-generated holes can transfer vertically through the nanosheet and reach to the Cl atom terminated surface to participate in oxidation reaction, while photo-generated electrons transfer to the opposite direction to participate in reduction reaction. Thereby, this is extremely advantageous for the process of photocatalytic reaction. Generally, the adsorption of dyes on the surface can reduce the polarity of the nanosheet. But after the photo-degradation of these dye molecules, newly produced species can escape the surface so that other dyes can be adsorbed on it, and this is a dynamic equilibrium process. In addition, because the nanosheet is very thin, the time used for transfer is much shorter than that of adsorption dyes. Therefore, the photo-generated electrons and holes can quickly transfer to the surface, and the presence of built-in electric field can accelerate this process. In order to further elucidate the mechanism of the transfer pathway of photo-generated carriers, a scheme is given in Fig 7. Because part of the excess electrons accumulated on the surface are removed after the creation of Bi vacancies, the positions of the VB and CB of the BiOCl nanosheet are gradually ascended from the Bi to Cl atomic termination, which facilitates the separation of charge carriers and may explain the great

improvement of photocatalytic activity observed experimentally.

Finally, using this novel slab model, we will provide an explanation for the band edge upshift for the ultrathin BiOCl nanosheets with respect to nanoplates observed by experiment. Considering the large thickness of nanoplates (about 30nm), we use the Bi1 surface (as shown in Fig 2a) to simulate the nanoplate because the properties in the middle of the slab is almost bulk-like. The band edge positions are determined via the alignment of average electrostatic potentials of these slabs with the vacuum level. As shown in Table 2, the VBM of ultrathin nanosheet is about 6.13 eV with respect to vacuum, which is similar to that of BiOCl nanoplate, indicating that the pure nanosheet does not show any significant upshift of band edges relative to the nanoplate. Since two Cl atomic layers are removed compared with the stoichiometry BiOCl slab, the surface of the nanoplate has the same electron density as the nanosheet. Thus, the similar surface environment leads to almost the same band edge positions. When one Bi atom is removed from the Bi terminated surface, corresponding the injection of three holes, the density of excess electrons at the Bi terminated surface is expected to be reduced, which can further lead to the enhanced polarity and ascend the band edge positions for this nanosheet. To confirm it, the average electrostatic potential of one Bi vacancy contained BiOCl nanosheet is calculated. We find that the value of VBM is 4.26 eV and the upshift is reach to 1.87 eV, which is significantly larger than the experimental observation.[35] It can be understood because the concentration of surface Bi vacancies of the ultrathin BiOCl (001) nanosheet synthesized by experiment may be smaller than this model. Moreover, the presence of the O vacancies in the surface may play a detrimental role. It is known that the CBM of BiOCl is a little more positive than the H^+/H_2 potential level (about 0.09 eV), this upshift of the CBM can lead to the ability of splitting water to produce hydrogen observed from the experiment.[42] Two Bi atoms are removed from the surface of nanosheet to further explore the origin of the band edge upshift, despite that the concentration of Bi vacancies in nanosheet synthesized by experiment is much lower than this slab model. The calculated value of VBM is 3.79 eV. In addition, for the Bi atom layer-resolved DOS, as shown in Fig 8a, no obvious change for the band

edges can be found compared with the case of one Bi vacancy contained nanosheet, we attribute it to the reduced cationic concentration for the Bi terminated surface, which is known to decrease the polarity of the surfaces.[41] To verify it, two Bi atoms are removed from the inner of the slab. The Bi atom layer-resolved DOS are given in Fig 8b, in which a conduction surface state can be found. This state will not be obtained in experiment because the extremely high formation energy prevents the formation of such high Bi vacancy concentration in bulk. Here, we employ this model only to explore the origin of band edge upshift for the nanosheet. We note that going from the top Bi layer to the 5 Bi layer, a large upshift can be realized due to the significantly enhanced polarity, but from the 6 to the 8 layers, a slightly downshift can be observed, we assign it to a local charge imbalance resulted from the vacancy induced lattice relaxation. Therefore, we believe that the presence of Bi vacancies in the surface of BiOCl (001) nanosheet is very important for the enhanced photocatalytic activity. It can not only increase the polarity of surface, but also provide large number places for the adsorption of organic dyes, which is favorable for photocatalytic reaction process.

Conclusion

In summary, we have studied the electronic structures and photocatalytic properties of the ultrathin BiOCl (001) nanosheet by employing density functional method. The surface energy implies that Cl2 atomic termination is more stable compared with others and tends to present on the surface of the ultrathin BiOCl (001) nanosheet. In addition, the Bi and O vacancies in the Bi terminated surface have significantly lower formation energies compared with the inner of the nanosheet, indicating that these defects are more likely to be introduced in surface, while the Cl vacancy does not have these properties. The lack of the polarity in pure BiOCl (001) nanosheet can be attributed to the excess electrons resulting from off-stoichiometric slab model. However, the presence of Bi vacancies in the Bi terminated surface can enhance polarity of nanosheet, which further leads to band blending and is extremely

advantageous for photocatalytic performance. Moreover, the band edge upshift can be found in Bi vacancy contained BiOCl (001) nanosheet with respect to nanoplate, which may render it the ability of splitting water to produce hydrogen.

Acknowledgement

This work is supported by the National Basic Research Program of China (973 prog ram, 2013CB632401), National Science foundation of China under Grant11374190, 2 1333006, and 11404187 and 111 Project B13029, and the Taishan Scholar Program of Shandong. We also thank the National Supercomputer Center in Jinan for providing high performance computation.

References

1. X. B. Chen, S. H. Shen, L. J. Guo and S. S. Mao. *Chem. Rev.*, 2010, **110**, 6503–6570.

2. H. Tong, S. Ouyang, Y. Bi, N. Umezawa, M. Oshikiri and J. Ye. *Adv. Mater.*, 2012, **24**, 229–251.

3. P. Wang, B. B. Huang, X. Y. Qin, X. Y. Zhang, Y. Dai, J. Y. Wei and M.-H. Whangbo, *Angew. Chem., Int. Ed.*, 2008, **47**, 7931–7933.

4. P. Wang, B. Huang, Y. Dai and M.-H. Whangbo, *Phys. Chem. Chem. Phys.*, 2012, **14**, 9813–4536.

5. H. Cheng, B. Huang, J. Lu, Z. Wang, B. Xu, X. Qin, X. Zhang and Y. Dai, *Phys. Chem. Chem. Phys.*, 2010, **12**, 15468–15475.

6.T. W. Kim and K.-S. Choi, *Science*, 2014, **343**, 990–994.

7. H. Cheng, B. Huang and Y. Dai, *Nanoscale*, 2014, **6**, 2009–2026.

8. T. Jing, Y. Dai, W. Wei, X. Ma and B. Huang, *Phys. Chem. Chem. Phys.*, 2014, **16**, 18596–18604.

9. K. L. Zhang, C. M. Liu, F. Q. Huang, C. Zheng and W. D. Wang, *Appl. Catal., B*, 2006, **68**, 125–129.

10. H. Cheng, B. B. Huang and Y. Dai, *Nanoscale*, 2014, **6**, 2009–2026.

11. J. Jiang , K. Zhao , X. Xiao , and L. Zhang, *J. Am. Chem. Soc.*, 2012, **134**, 4473–4476.

12. T. B. Li , G. Chen , C. Zhou , Z. Y. Shen , R. C. Jin and J. X. Sun, *Dalton Trans.*, 2011, **40**, 6751–6758.

13. H. Zhang, L. Liu and Z. Zhou, *Chem. Chem. Phys.*, 2012, **14**, 1286–1292.

14. X. Zhang, B. Li, J. Wang, Y. Yuan, Q. Zhang, Z. Gao, L. M. Liu and L. Chen, *Phys. Chem. Chem. Phys.*, 2014, **16,** 25854–25861.

15. X. Zhang, C. Fan, Y. Wanga, Y. Wanga, Z. Liang and P. Han, *Computational Materials Science*, 2013, **71**, 135–145.

16. H. Gnayem and Y. Sasson, ACS Cata*l.*, 2013, **3**, 861–861.

17. J. Jiang, L. Zhang, H. Li, W. He and J. J. Yin, *Nanoscale*, 2013, **5**, 10573-10581.

18. K. Zhang, D. Zhang, J. Liu, K.Ren, H. Luo, Y. Peng, G. Li and X. Yu, *CrystEngComm*, 2012, **14**, 700–707.

19. X. Zhang, L. Zhao, C. Fan, Z. Liang, P. Hanb, *Physica B: Condensed Matter*, 2012, **407**, 4416–4424.

20. L. Ye , L. Zan, L. Tian, T. Peng and J. Zhang, *Chem. Commun.*, 2011, **47**, 6951–6953.

21. L. Ye, K. Deng , F. Xu, L. Tian , T. Peng and L. Zan, *Phys. Chem. Chem. Phys.*, 2012, **14**, 82–85.

22. W. Yang, Y. Wen, R. Chen, D. Zeng and B. Shan, Phys. *Chem. Chem. Phys.*, 2014, **16**, 21349–21355.

23. J. Li , K. Zhao, Y. Yu and L. Zhang, *Adv. Funct. Mater.*, 2015, **25**, 2189–2201.

24. Y. Okamoto, S. Ida, J. Hyodo, H. Hagiwara, and T. Ishihara, *J. Am. Chem. Soc.*, 2011, **133**, 18034–18037.

25. S. Ida, A. Takashiba, S. Koga, H. Hagiwara and T. Ishihara, *J. Am. Chem. Soc.*, 2014, **136**, 1872−1878.

26. J. Zhu, Z. Yin, D. Yang, T. Sun, H. Yu, H. E. Hoster, H. H. Hng, H. Zhang and Q. Yan, *Energy Environ. Sci.*, 2013, **6**, 987−993.

27. W. Zhou, Z. Yin, Y. Du, X. Huang, Z. Zeng, Z. Fan, H. Liu, J. Wang and H. Zhang,

Small, 2013, **9**, 140−147.

28. L. Ye, L. Zan, L. Tian, T. Penga and J. Zhang, *Chem. Commun.*, 2011, **47**, 6951–6953.

29. S. Weng, Z. Fang, Z. Wang, Z. Zheng, W. Feng and P. Liu, *ACS Appl. Mater. Interfaces*, 2014, **6**, 18423−18428.

30. X. Zhang, X. Bo Wang, L. W. Wang, W. K. Wang, L. L. Long, W. W. Li and H. Q. Yu, *ACS Appl. Mater. Interfaces*, 2014, **6**, 7766−7772.

31. H. Li, J. Shi, K. Zhao and L. Zhang, *Nanoscale*, 2014, **6**, 14168–14173.

32. J. Jiang, K. Zhao, X. Xiao and L. Zhang, *J. Am. Chem. Soc.*, 2012, **134**, 4473–4476.

33. K. Zhao, L. Zhang, J. Wang, Q. Li, W. He, and J. J. Yin, *J. Am. Chem. Soc.*, 2013, **135**, 15750−15753.

34. H. Zhang, L. Liu and Z. Zhou, *RSC Adv.*, 2012, **2**, 9224–9229.

35. M. Guan, C. Xiao, J. Zhang, S. Fan, R. An, Q. Cheng, J. Xie, M. Zhou, B. Ye and Y. Xie, *J. Am. Chem. Soc.*, 2013, **135**, 10411−10417.

36. L. Liao, Q. Zhang, Z. Su, Z. Zhao, Y. Wang, Y. Li, X. Lu, D. Wei, G. Feng, Q. Yu, X. Cai, J. Zhao, Z. Ren, H. Fang, F. Robles-Hernandez, S. Baldelli and J. Bao, *Nature Nanotechnology*, 2014, **9**, 69–73.

37. V. S. Kumar and M. K. Niranjan, *J. Appl. Phys.*, 2014, **115**, 173705.

38. L. Wang, J. Ge, A. Wang, M. Deng, X. Wang, S. Bai, R. Li, J. Jiang, Q. Zhang, Y. Luo and Y. Xiong, *Angew. Chem. Int. Ed.*, 2014, **53**, 5107–5111.

39. J. P. Perdew, J. Chevary, S. H. Vosko, K. A. Jackson, M. R. Pederson and D. J. Sing, *Phys. Rev. B: Condens. Matter Mater. Phys.*, 1992, **46**, 6671–6687.

40. H. G. Yang, C. H. Sun, S. Z. Qiao, J. Zou, G. Liu, S. C. Smith, H. M. Cheng, G. Q. Lu, *Nature*, 2008, **453**, 638−641.

41. J. Xiao, A. Kuc, T. Frauenheim and T. Heine, *Phys. Rev. Lett.*, 2014, **112**, 106102.

42. L. Zhang, Z. Han, W. Wang, X. Li, Y. Su, D. Jiang, X. Lei, and S. Sun, *Chem. Eur. J.*, 2015, **21**, 1−7.

Table 1 The thickness of different atomic terminated BiOCl (001) nanosheet. Experimental data is taken from Ref. 35.

Nanosheet	Bi1-Bi1	Bi1-Cl2	Bi-Cl1	Bi-O	Bi1-Bi2	Experiment
Thickness(Å)	24.81	26.49	28.56	30.70	31.07	27

Table 2 The positions of the VBM with respect to vacuum level for pure BiOCl nanoplate (Np), nanosheet (Ns), one Bi vacancy contained nanosheet and two Bi vacancies contained nanosheet.

BiOCl	Np(pure)	Ns (pure)	Ns(Bi_V)	Ns($2Bi_V$)
VBM(eV)	6.09	6.13	4.26	3.79

Figure Captions

Figure 1 The allowed chemical potential ranges (shaded region) under equilibrium growth conditions for BiOCl, A and D refer to the Bi-poor condition, B and C refer to the Bi-rich condition.

Figure 2 The crystal structure of BiOCl (a), the slab models employed for the surface energy calculation, Bi1 terminated (b), Bi2 terminated (c), O terminated (d), Cl1 terminated (e) and Cl2 terminated (f) BiOCl (001) surfaces.

Figure 3 The slab models employed for the cleavage energy calculation of nanosheets, Bi1-Bi1 (a), Bi1-Cl2 (b), Bi1-Cl1 (c), Bi1-Bi2 (d) and Bi1-O (e) refer to the slabs with one side terminated by Bi1 atoms and the other side terminated by Bi1, Cl2, Cl1, Bi2 and O atoms, respectively.

Figure 4 The calculated surface energies for various atomic terminated BiOCl (001) surfaces (a) and cleavage energies for various atomic terminated BiOCl (001) nanosheets (b) under four chemical potentials conditions.

Figure 5 The defect formation energies of Bi_V, O_V, and Cl_V in different layers for BiOCl (001) nanosheet.

Figure 6 The Bi atom layer-resolved PDOS of the defect free (a) and one Bi vacancy contained (b) BiOCl nanosheet.

Figure 7 The schematic of charge carrier separation for BiOCl (001) nanosheet.

Figure 8 The Bi atom layer-resolved PDOS with two Bi vacancies in the surface (a)

and inner(b) of BiOCl nanosheet.

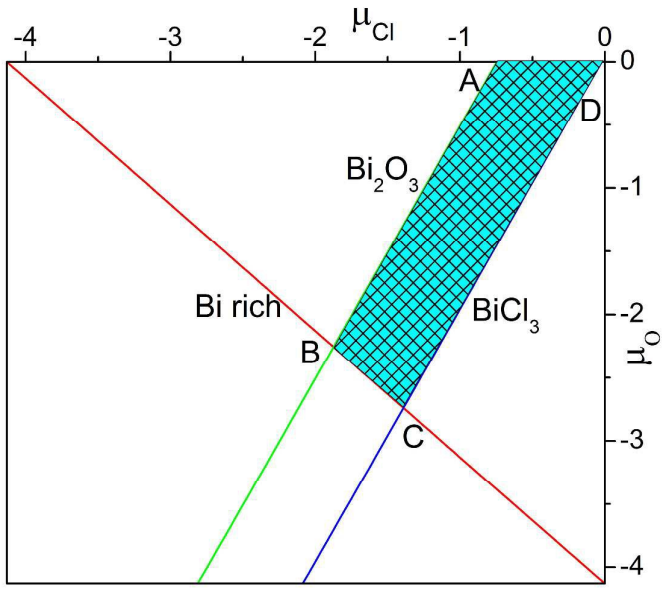

Figure 1

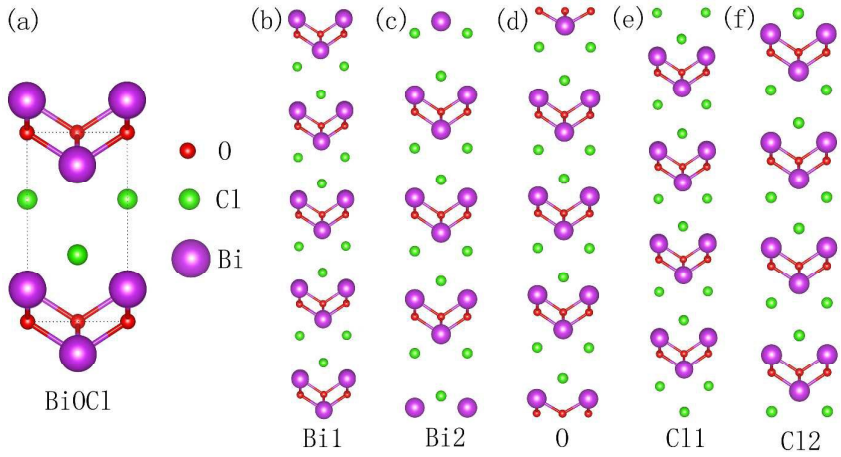

Figure 2

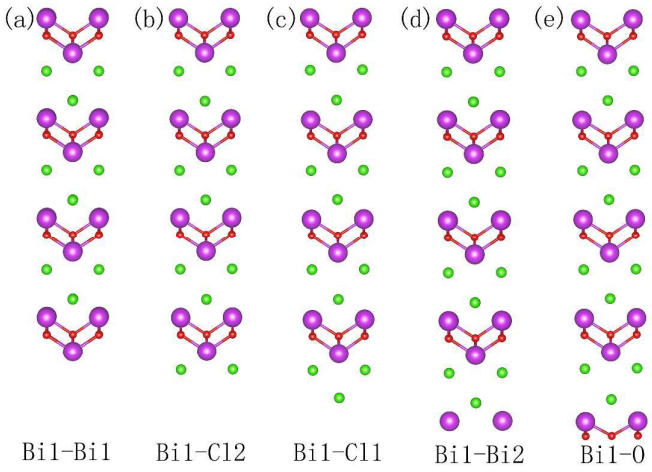

Figure 3

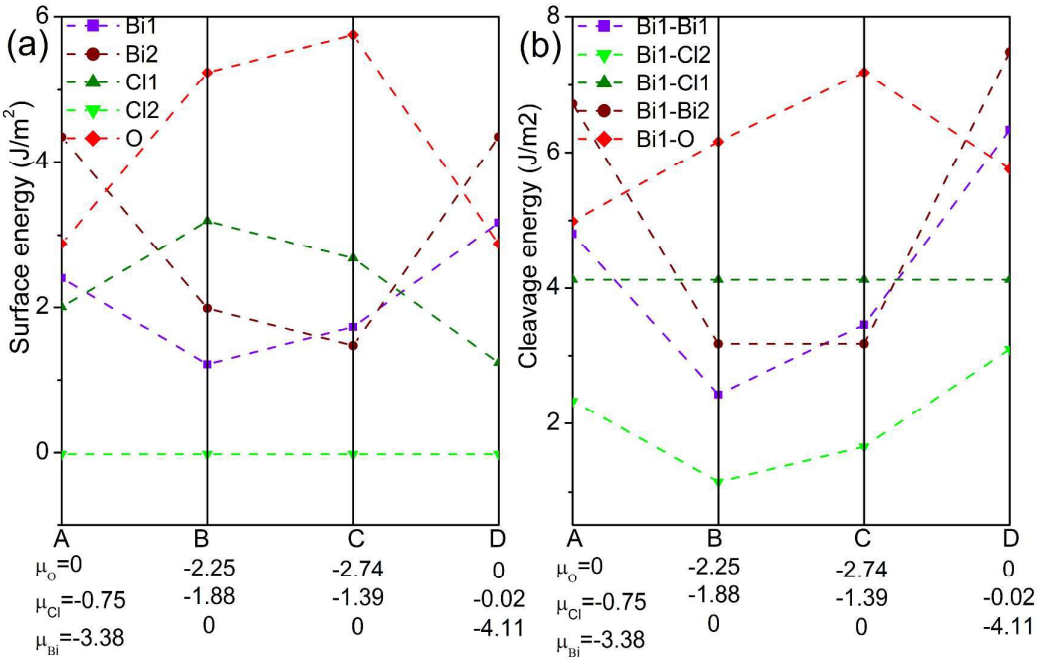

Figure 4

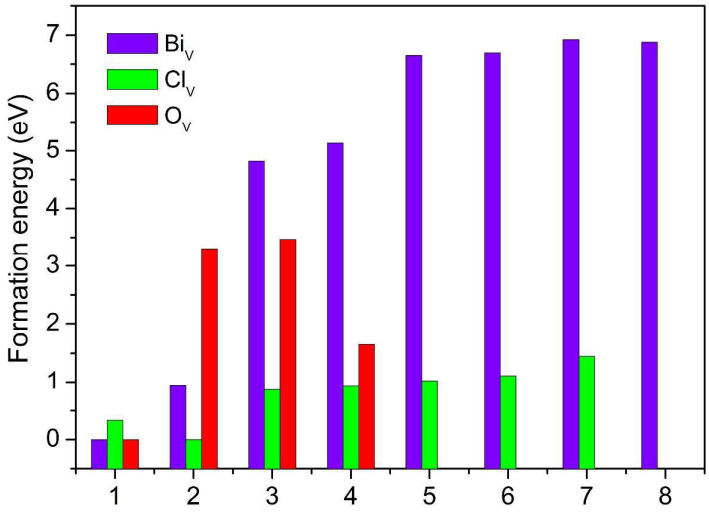

Figure 5

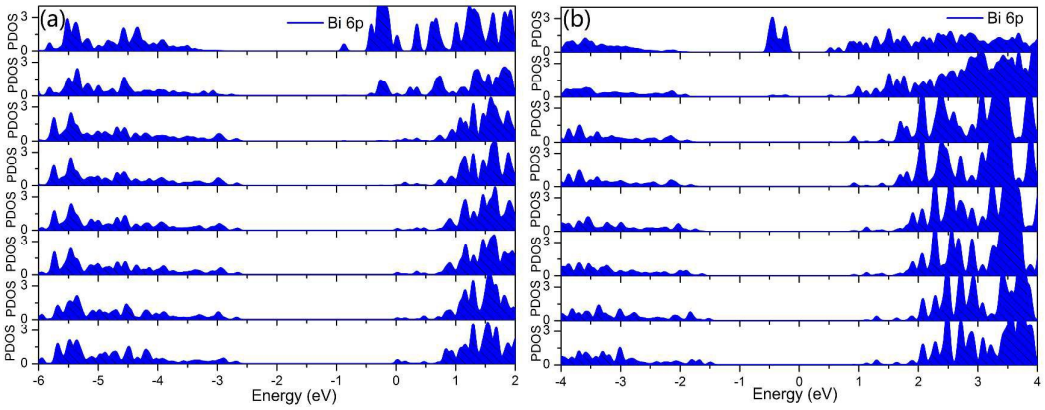

Figure 6

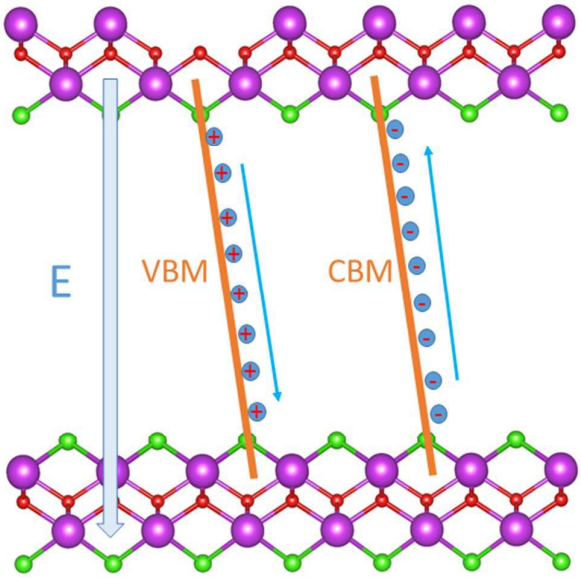

Figure 7

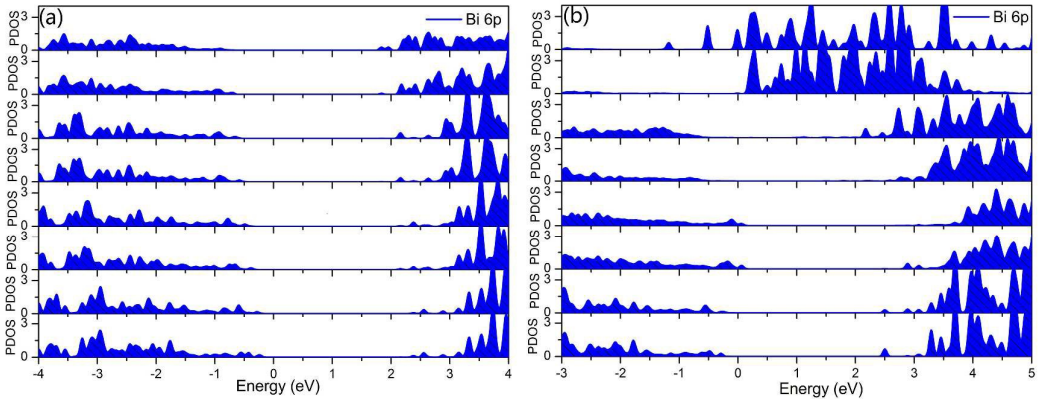

Figure 8